Supporting Information

Two Novel Lanthanide Metal-Organic Frameworks Based on Tetraphenylethylene for Ultra-High Proton Conduction

Qi Wu[a], Qianxi Li[a], Wenkang Zou[a], Zheyu Zhang[a], Yan Zhou[a]* and Qihua Zhao[ab]*

[a]School of Chemical Science and Technology, Yunnan University, Kunming 650500, P. R. China.

[b]Key Laboratory of Medicinal Chemistry for Natural Resource Education Ministry, Yunnan University, Kunming 650091, P. R. China.

Corresponding Authors. E-mail: yanzhou@ynu.edu.cn, qhzhao@ynu.edu.cn.

Table of contents

EXPERIMENTAL SECTION

Materials and Apparatus

All chemical reagents were commercially available without further purification, including europium chloride hexahydrate ($EuCl_3 \cdot 6H_2O$), dysprosium nitrate hexahydrate ($Dy(NO_3)_3 \cdot 6H_2O$), *N, N*-dimethylformamide (DMF) and trifluoroacetic acid (TFA). The ligand H_4TCBPE-F can be synthesized according to the literature.[1]

With using Bruker AXS CCD D8 VENTURE, Single crystal X-ray diffraction was performed with Cu Kα radiation. Powder X-ray diffraction (PXRD) was performed using the Rigaku TTRIII-18KW diffractometer (Rigaku, Japan) with Cu Kα radiation and an angular range of 3-50° (2θ). Fourier transform infrared spectroscopy (FT-IR) is measured with a Fourier transform infrared spectrophotometer (Nicoletis 10), and the crystal sample is ground with KBr and pressed into thin sheets for testing in the test range of 4000-400 cm^{-1}. In Ar atmosphere, Thermogravimetric analysis (TGA) is performed on a Mettler Tolli synchronous differential thermal analyzer (30-800°C, heating rate 10°C/min). The water vapor adsorption experiments were carried out with the Quantachrome Autosorb IQ (USA) device at different relative humidity levels at 25°C. Before measuring water absorption, the two samples were activated for 12 h under vacuum at 120°C.

Synthesis of Ln-MOFs

In a 15 mL rigid pressure-resistant glass tube, H_4TCBPE-F (5.0 mg, 0.006 mmol) and $EuCl_3 \cdot 6H_2O$ (10.0 mg, 0.066 mmol) were weighed and added sequentially, followed by the addition of 2.0 mL of DMF and 0.15 mL of TFA. The mixture was heated to 60°C for 72 h and then allowed to cool naturally to room temperature. Yellow-green needle-like crystals were obtained and washed with DMF several times. Yield: 60% (calculated based on H_4TCBPE-F). Infrared spectral test data (FT-IR, KBr, cm^{-1}): 3423 (m), 2924 (w), 2854 (w), 1621 (s), 1589 (s), 1383 (m), 1188 (w), 1109 (m), 906 (w), 865 (w), 833 (w), 787 (m), 698(w), 622(w), 516(w).

The preparation method of **Dy-MOF** is similar to the **Eu-MOF**, except that

$Dy(NO_3)_3 \cdot 6H_2O$ is used instead of $EuCl_3 \cdot 6H_2O$. The relevant measurement data are as follows:

Dy-MOF: Yield: 60% (calculated based on H_4TCBPE-F). Infrared spectral test data (FT-IR, KBr, cm^{-1}): 3421 (m), 2924 (w), 2854 (w), 1618 (s), 1587 (s), 1384 (m), 1188 (w), 1108 (m), 904 (w), 866 (w), 831 (w), 790 (m), 698 (w), 622 (w), 556 (w).

The X-ray crystallographic coordinates for structures reported in this Article have been deposited at the Cambridge Crystallographic Data Centre (CCDC), under deposition number CCDC 2381005 and CCDC for 2385883 compound **Eu-MOF** and **Dy-MOF**. These data can be obtained free of charge from the Cambridge Crystallographic Data Centre via www.ccdc.cam.ac.uk/data_request/cif. All relevant data supporting the findings of this study are available from the corresponding authors on request.

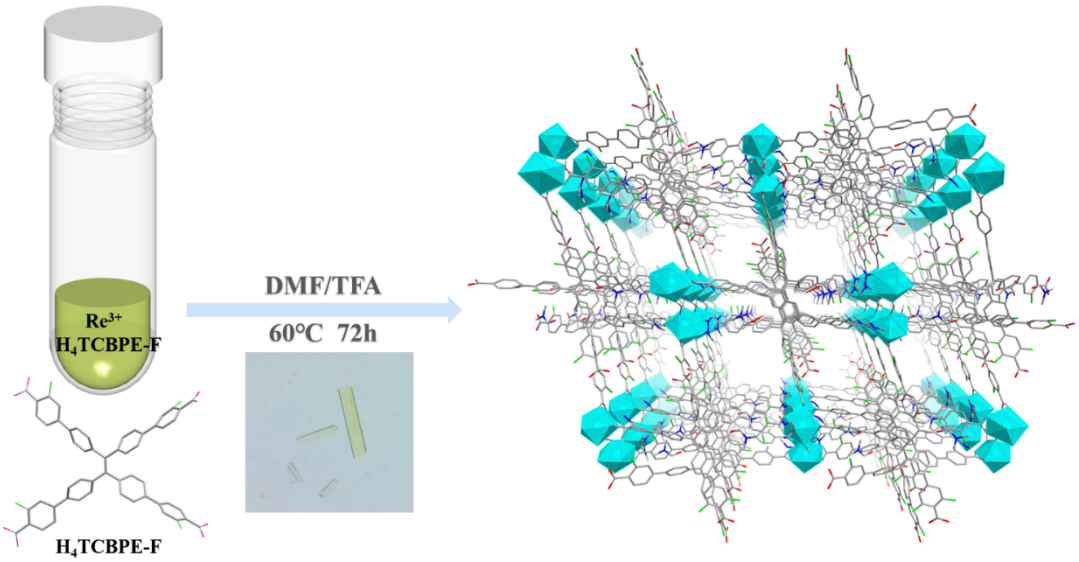

Scheme 1. Schematic of Syntheses and Optical Images of **Eu-MOF** and **Dy-MOF**.

Stability Experiment

Crystal samples of **Eu-MOF** and **Dy-MOF** were immersed in water, and the water-soaked MOF was subsequently dried at 50°C to obtain PXRD. Next, the MOF samples were immersed in acidic (pH=1, 3, 5) or alkaline (pH=9, 11, 13) solutions, and then soaked MOF was dried at 50°C and the PXRD pattern was obtained to detect the stability of **Eu-MOF** and **Dy-MOF**.

Proton Conductivity Measurement

For all proton conductivity measurements, electrochemical impedance spectra were recorded by Shanghai Chenhua CHI660E electrochemical workstation software. The temperature range was from 30 to 90°C, the frequency range was from 1 Hz to 1 MHz and the relative humidity is 68%, 75%, 85%, 93%, 98%. Then, about 30 mg of **Eu-MOF** and **Dy-MOF** powder were weighed and placed in a mold with a diameter of 5 mm, and the fixed samples (average diameter of 5.05 mm, thickness of 1.10 mm) obtained by pressing at 5 MPa for 5 min and were sandwiched between two Cu electrodes. Then the circular sheet was connected to the electrochemical workstation through the quasi-four-probe system. In order to obtain more accurate electrochemical data, the samples were stabilized at different humidity levels for a period of time before starting the test. These circular flakes were then telescoped in a constant humidity thermostat under the conditions described above for testing.

Proton conductivity (σ, $S \cdot cm^{-1}$) was calculated using the equation[2]

$$\sigma = \frac{L}{RS} \tag{1}$$

where L (cm), R (Ω), S (cm^2) are the thickness, measured impedance and surface area of the particle.

The activation energy E_a (eV) is calculated from the Arrhenius equation.[3,4]

$$\sigma T = \sigma_0 exp\left(\frac{-E_a}{kT}\right) \tag{2}$$

Where σ is the conductivity ($S \cdot cm^{-1}$), T (K) is the absolute temperature and k is the Boltzmann constant, 8.6×10^{-5} $eV \cdot K^{-1}$.

Analysis of Impedance Simulation Diagram

Equivalent circuits for the Nyquist plots of **Eu-MOF** and **Dy-MOF** at 30°C and 90°C and 98% relative humidity were fitted by the Nova2 program (Figure S22-S23).

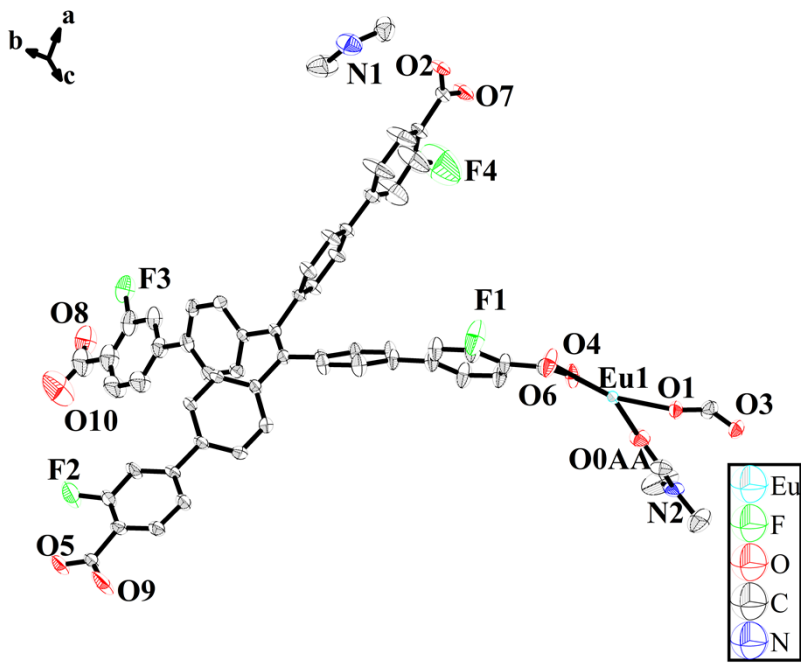

Fig. S1. The minimum asymmetric unit ellipsoid diagram of the **Eu-MOF**.

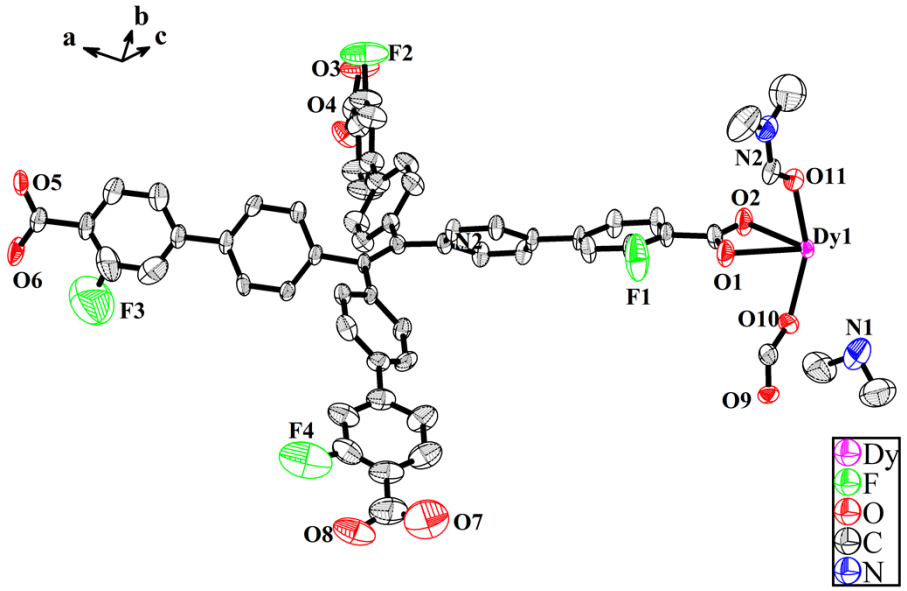

Fig. S2. The minimum asymmetric unit ellipsoid diagram of the **Dy-MOF**.

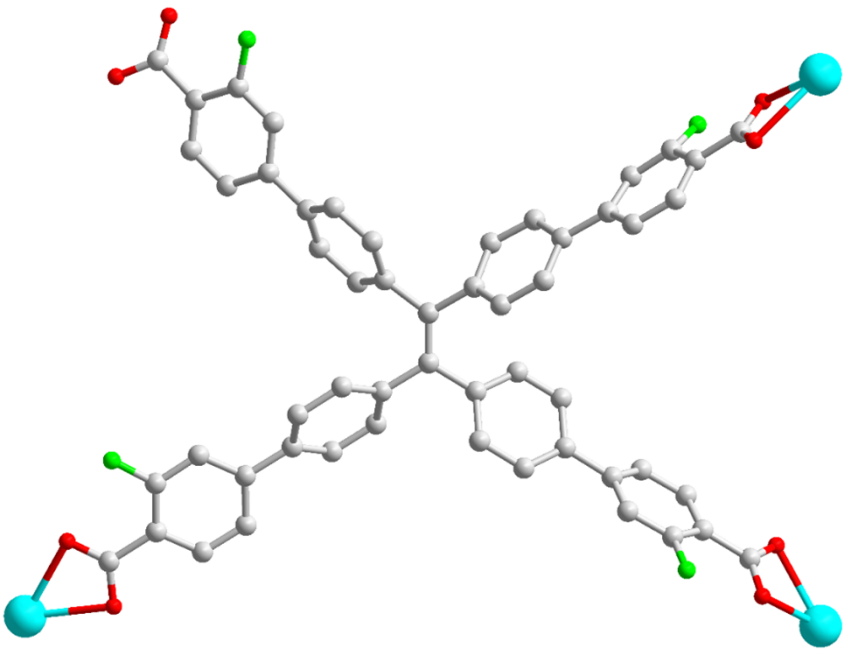

Fig. S3. The coordination environment of the ligand in **Eu-MOF** and **Dy-MOF**, for clear visibility, the hydrogen atom has been omitted.

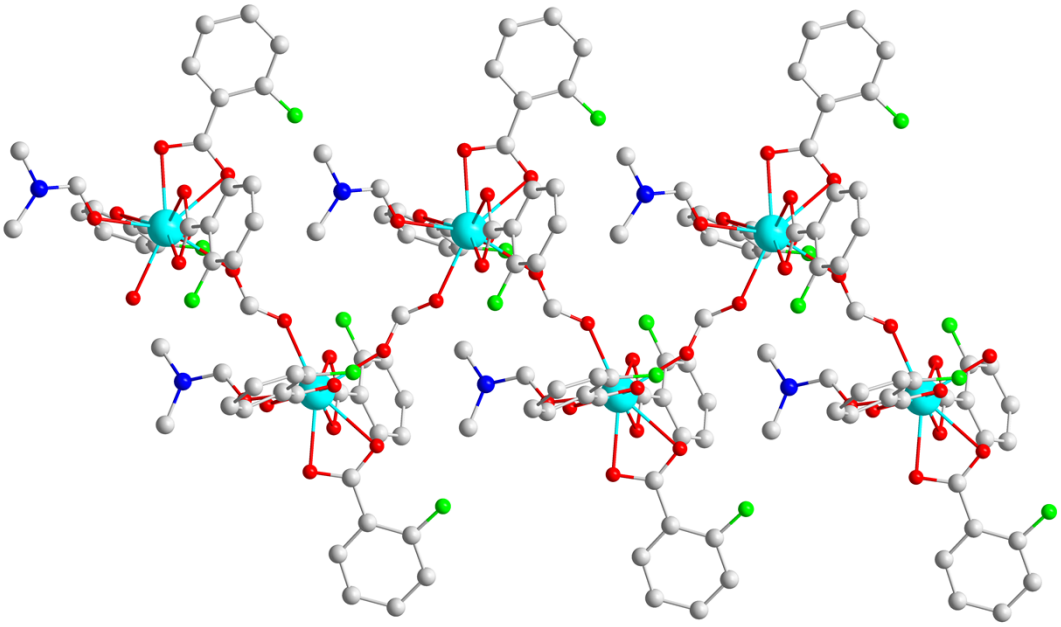

Fig. S4. Coordination environment of the middle metal atom of **Eu-MOF**.

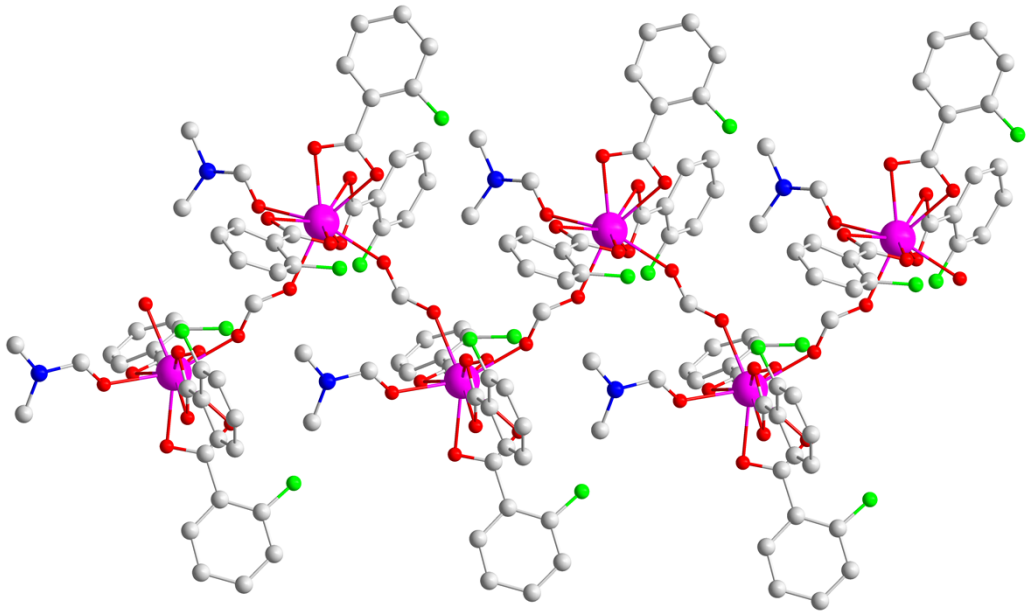

Fig. S5. Coordination environment of the middle metal atom of **Dy-MOF**.

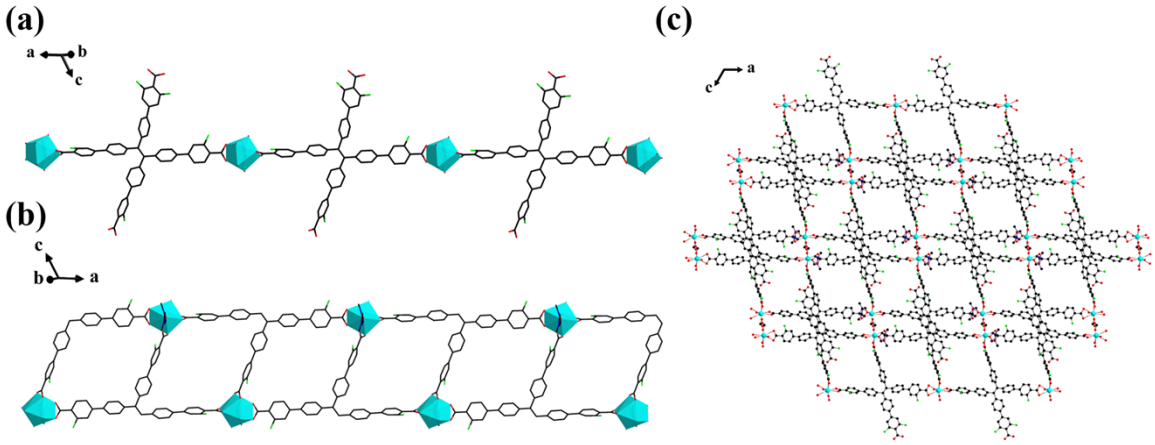

Fig. S6. (a) 1D chain-like structure connected by H_4TCBPE-F of **Ln-MOF**; (b) The two-dimensional face of the **Ln-MOF**; (c) 3D stacking diagram of the **Ln-MOF**.

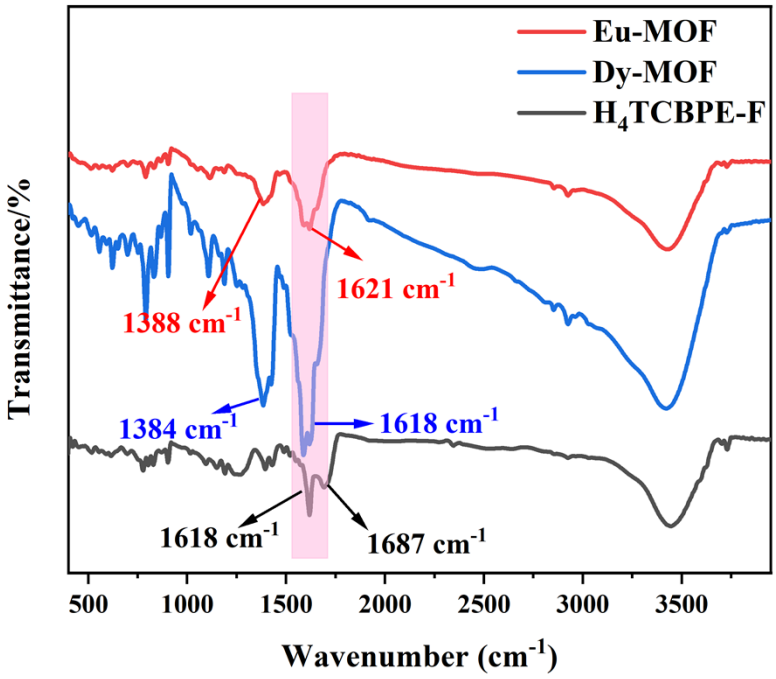

Fig. S7. FT-IR spectra of **Eu-MOF** and **Dy-MOF**.

By FT-IR test, we obtained that at around 3500 cm^{-1}, the large and broad peak be caused by the stretching vibration of -OH in water molecules. The vibrational absorption peaks in $[Me_2NH_2]^+$ at ν(N-H) 2852 cm^{-1} , ν(C-N) 1388 cm^{-1} and ν(C-H) at 2925 cm^{-1} were found. ν(C=O) at 1687 cm^{-1} disappeared in **Ln-MOF**, which suggests that there is a coordination interaction between -COOH in H_4TCBPE-F and the metal have coordination interactions. And the vibrational absorption peaks at ν(C=C) 1618 and 1621 cm^{-1} in the ligand H_4TCBPE-F were observed in **Eu-MOF** and **Dy-MOF**.

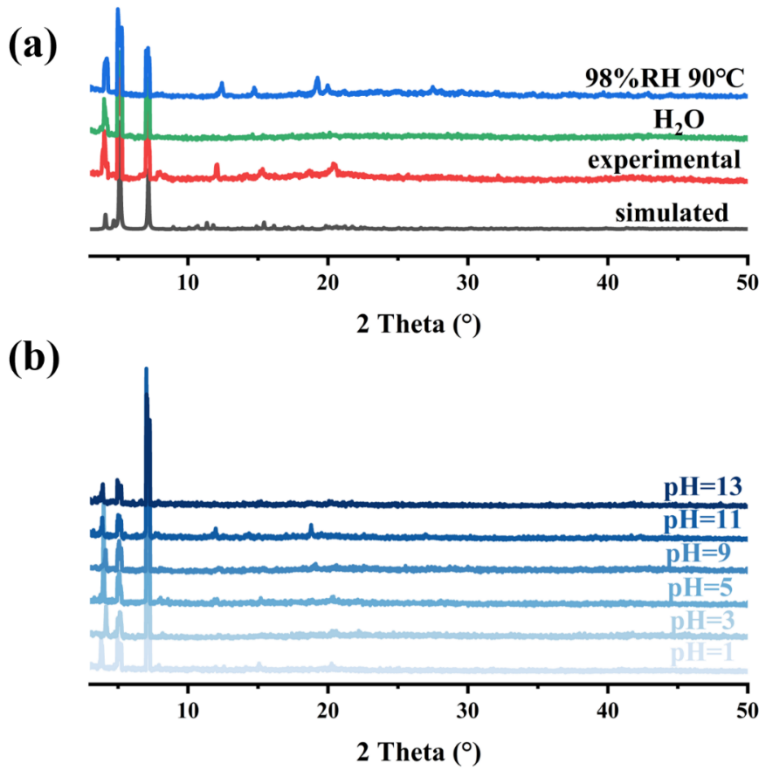

Fig. S8. (a) PXRD of **Eu-MOF** after immersion in water and electrochemical testing at 98% RH and 90°C; **(b)** PXRD of **Eu-MOF** in different pH aqueous solution.

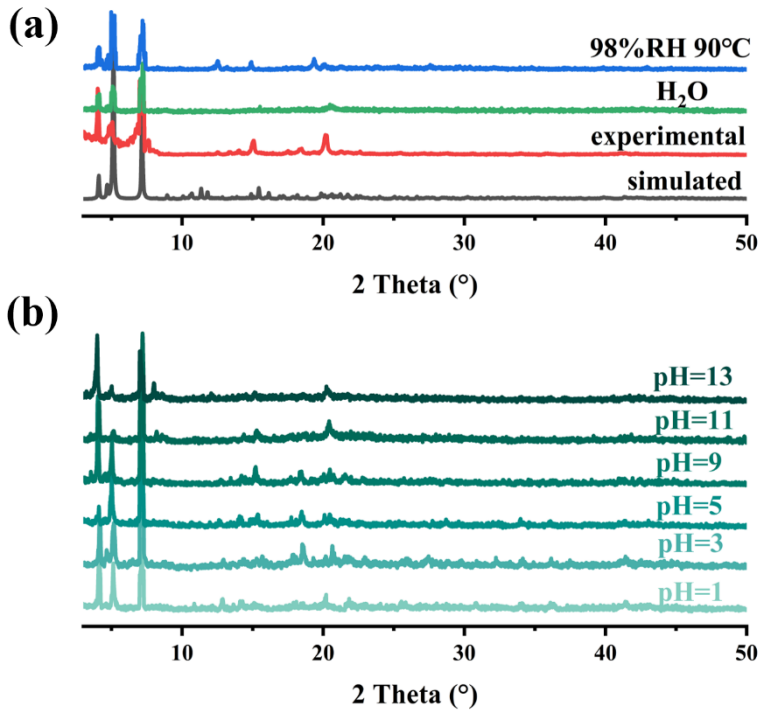

Fig. S9. (a) PXRD of **Dy-MOF** after immersion in water and electrochemical testing at 98% RH and 90°C; **(b)** PXRD of **Dy-MOF** in different pH aqueous solution.

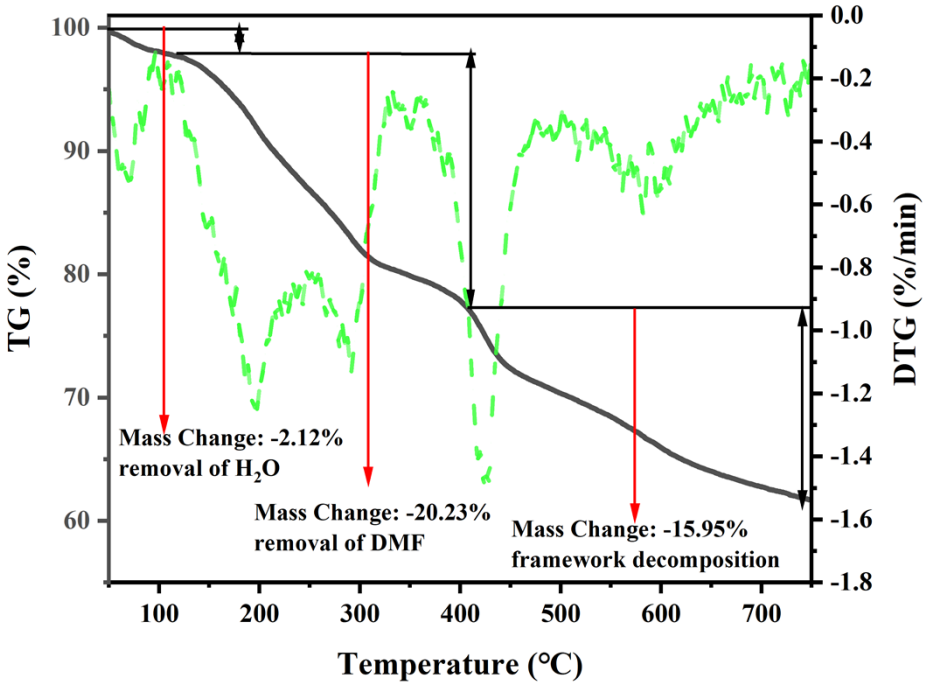

Fig. S10. Thermogravimetric analysis (TGA) and micro-quotient thermogravimetric curves (DTG) of **Eu-MOF** in Ar atmosphere.

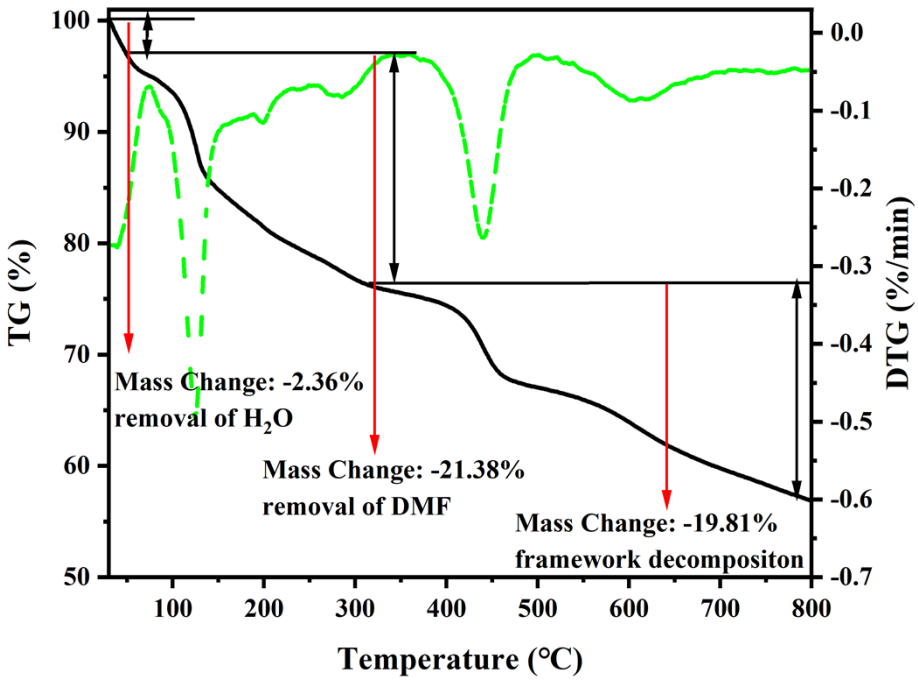

Fig. S11. Thermogravimetric analysis (TGA) and micro-quotient thermogravimetric curves (DTG) of **Dy-MOF** in Ar atmosphere.

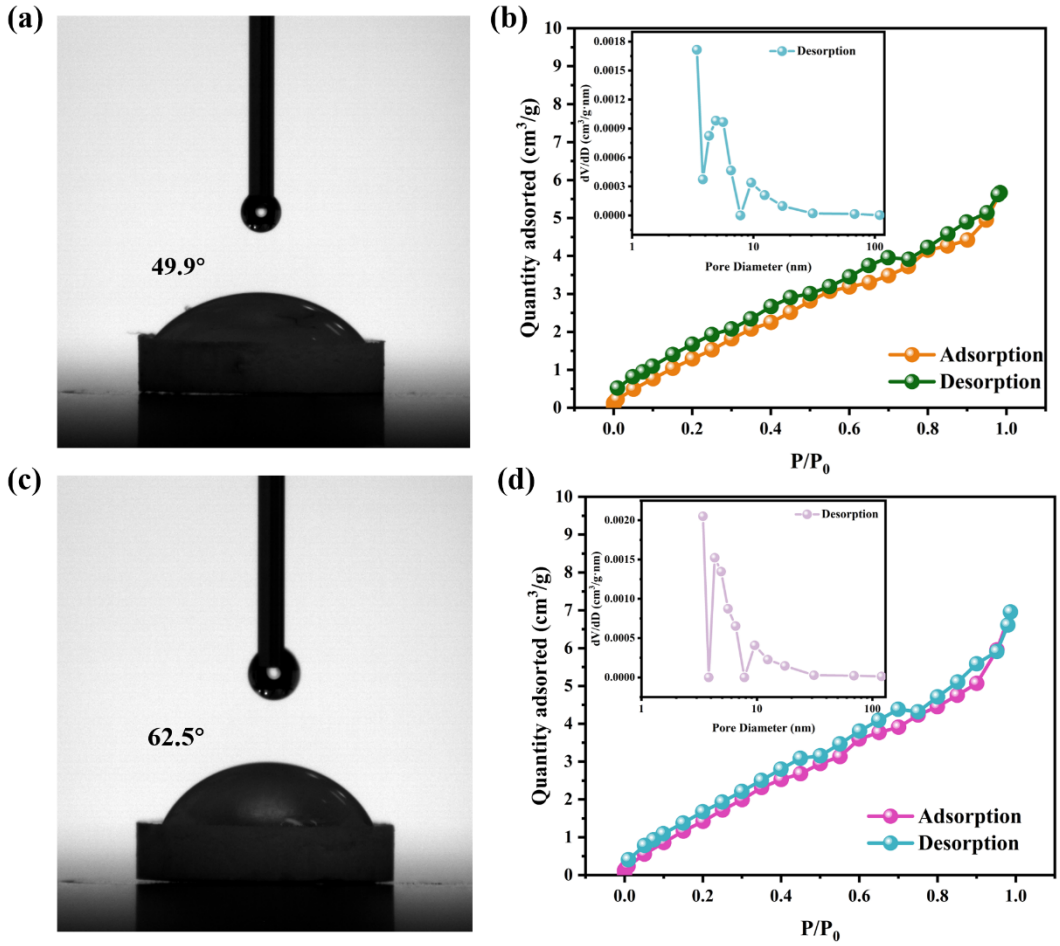

Fig. S12. (a) Water contact angle of **Eu-MOF**; (b) N_2 adsorption-desorption isotherms of **Eu-MOF**; (c) Water contact angle of **Dy-MOF**; (d) N_2 adsorption-desorption isotherms of **Dy-MOF**.

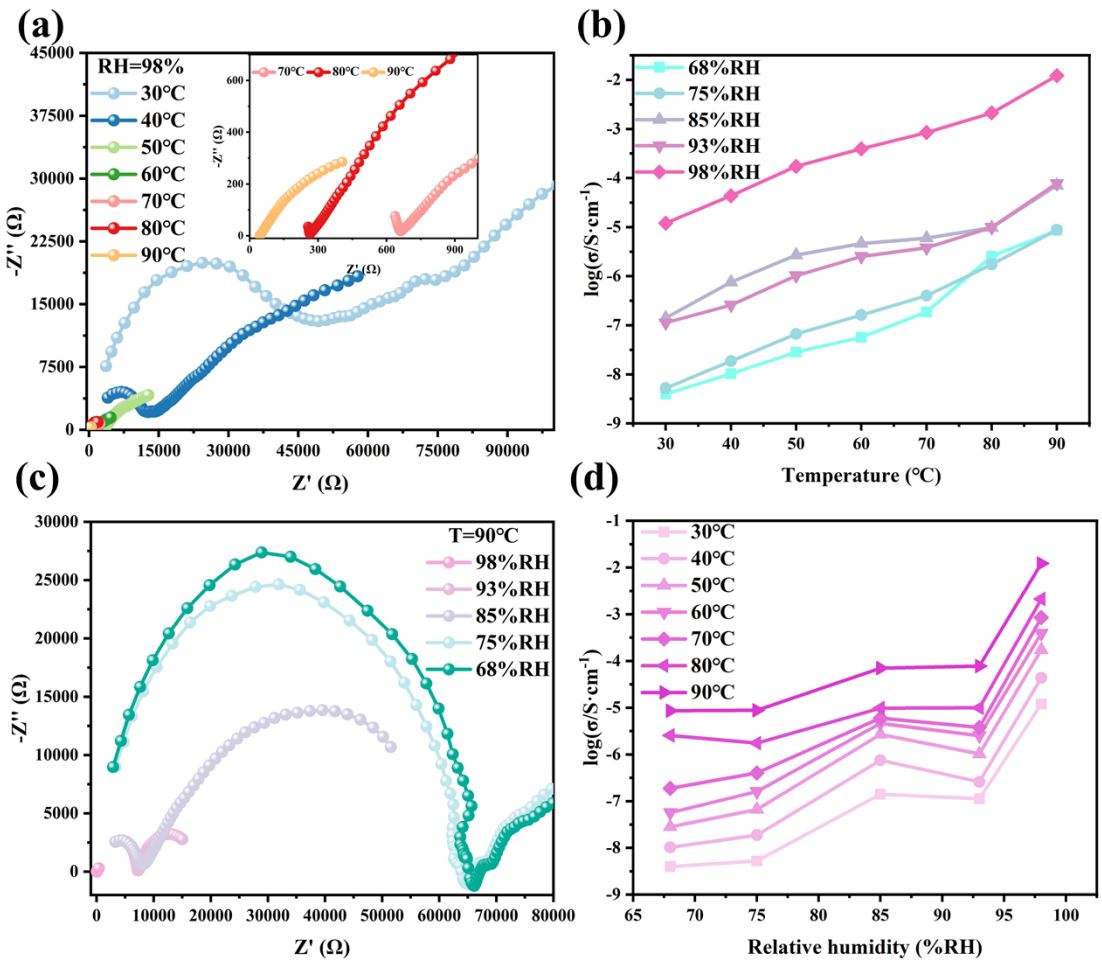

Fig. S13. (a) Nyquist plot of proton conductivity of **Dy-MOF** at 30-90°C and 98% RH; (b) **Dy-MOF** of temperature dependence plots; (c) Nyquist plot of the proton conductivity of **Dy-MOF** at 90°C and different humidity; (d) Plot of the humidity dependence of the **Dy-MOF**.

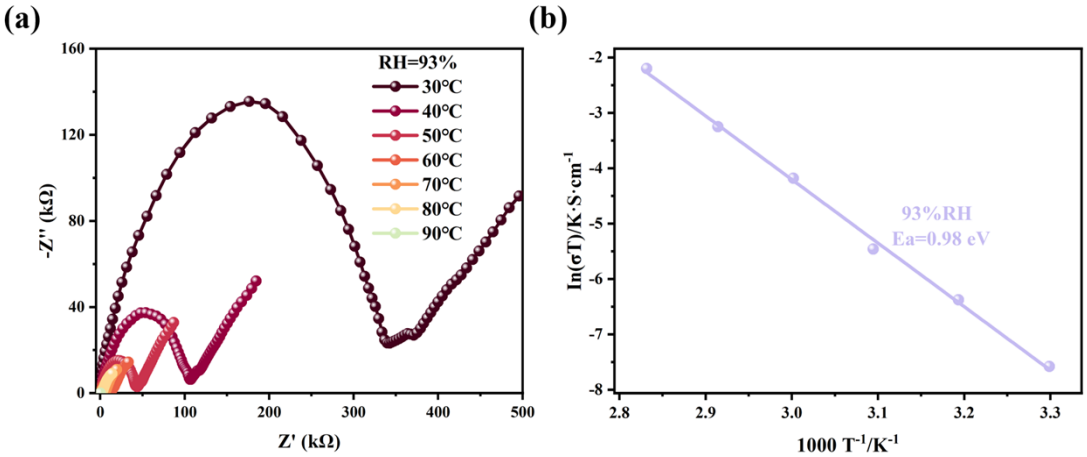

Fig. S14. (a) Nyquist plot of proton conductivity of **Eu-MOF** at 30-90°C (93% RH); (b) Arrhenius of **Eu-MOF** at 93% RH.

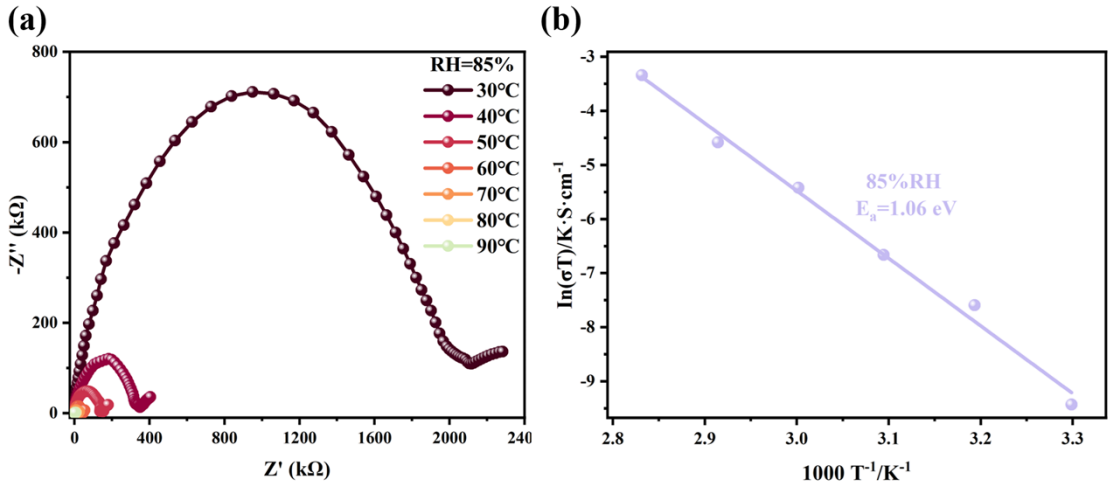

Fig. S15. (a) Nyquist plot of proton conductivity of **Eu-MOF** at 30-90°C (85% RH); (b) Arrhenius of **Eu-MOF** at 85% RH.

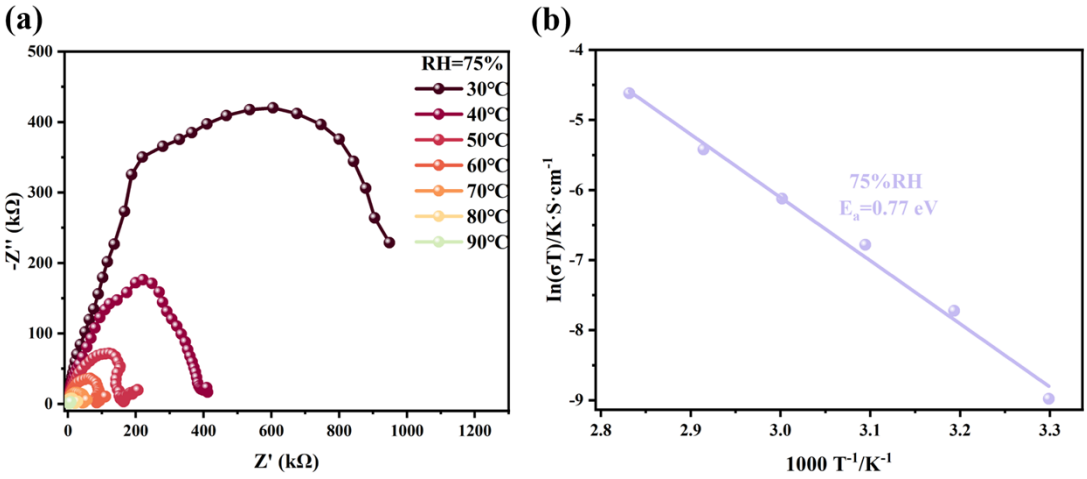

Fig. S16. (a) Nyquist plot of proton conductivity of **Eu-MOF** at 30-90°C (75% RH); (b) Arrhenius of **Eu-MOF** at 75% RH.

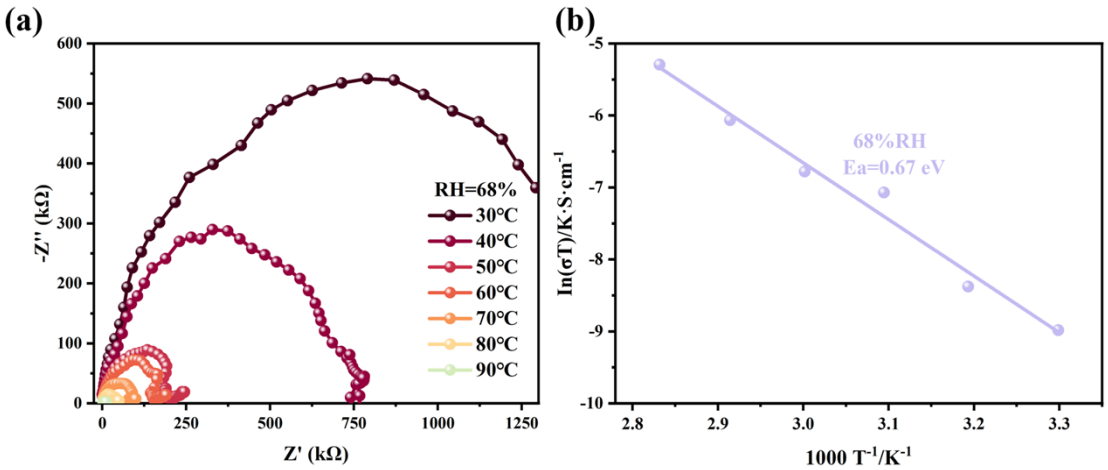

Fig. S17. (a) Nyquist plot of proton conductivity of **Eu-MOF** at 30-90°C (68% RH); (b) Arrhenius of **Eu-MOF** at 68% RH.

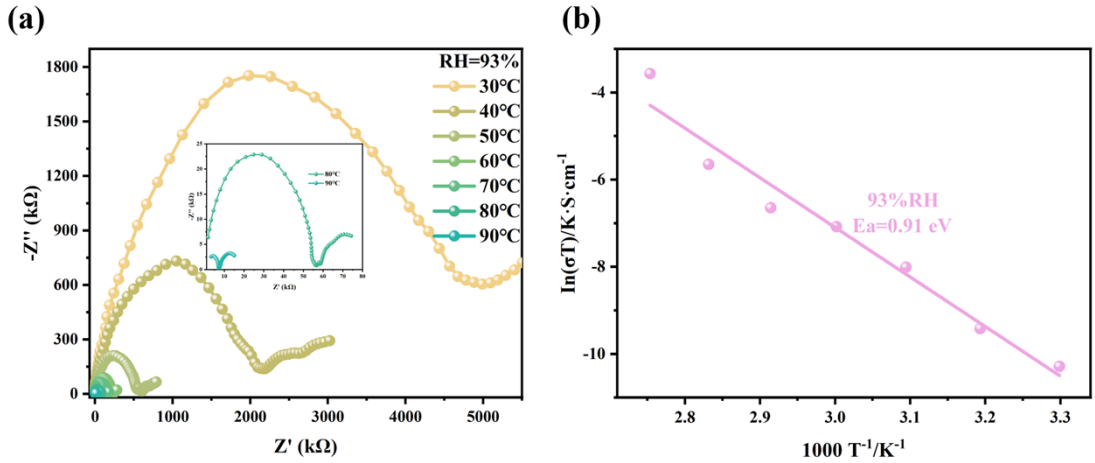

Fig. S18. (a) Nyquist plot of proton conductivity of **Dy-MOF** at 30-90°C (93% RH); (b) Arrhenius of **Dy-MOF** at 93% RH.

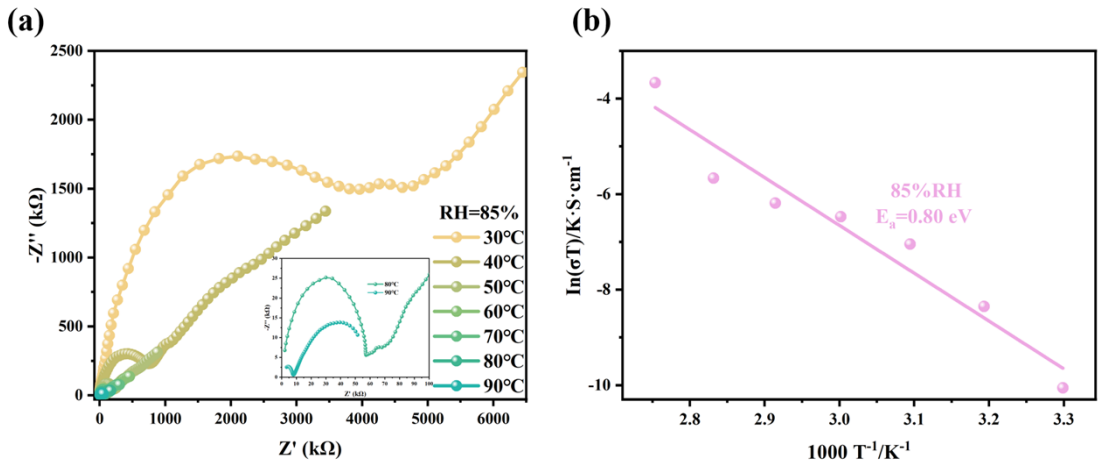

Fig. S19. (a) Nyquist plot of proton conductivity of **Dy-MOF** at 30-90°C (85% RH); (b) Arrhenius of **Dy-MOF** at 85% RH.

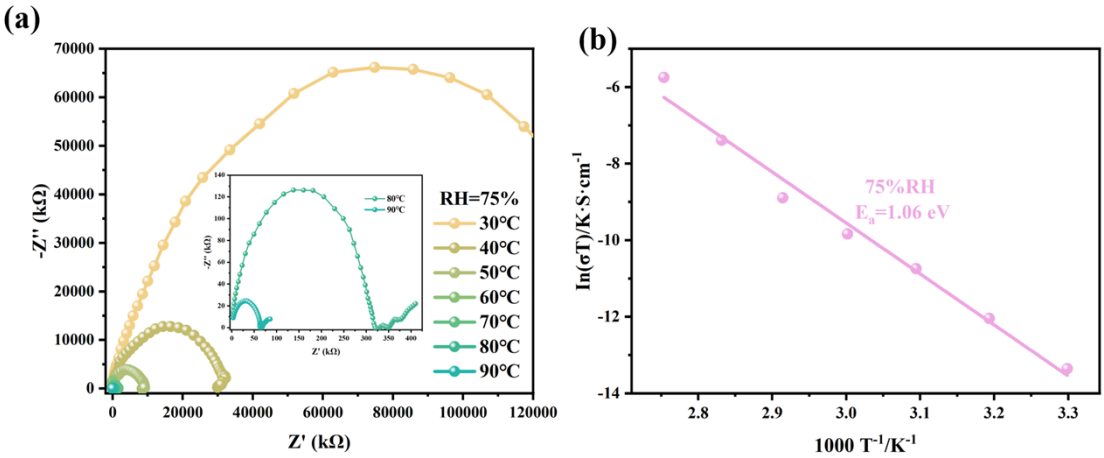

Fig. S20. (a) Nyquist plot of proton conductivity of **Dy-MOF** at 30-90°C (75% RH); (b) Arrhenius of **Dy-MOF** at 75% RH.

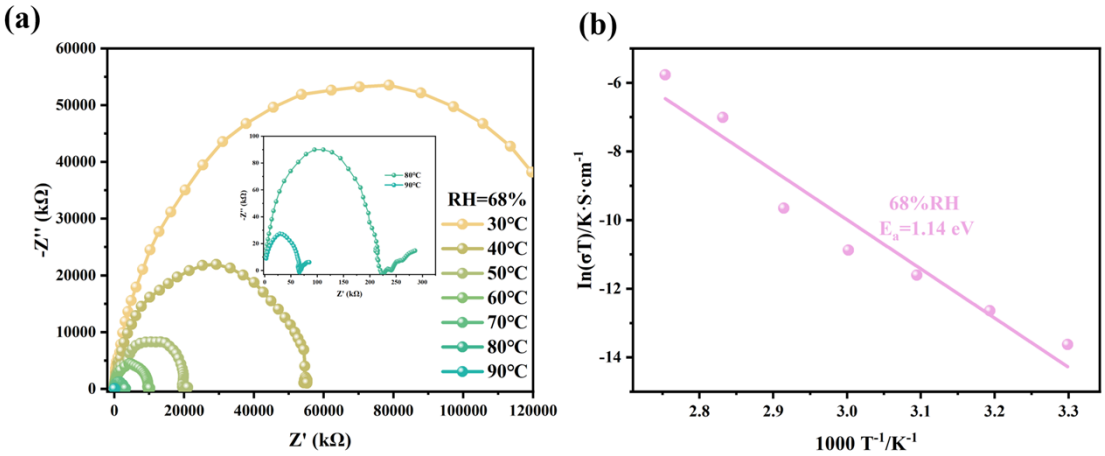

Fig. S21. (a) Nyquist plot of proton conductivity of **Dy-MOF** at 30-90°C (68% RH); (b) Arrhenius of **Dy-MOF** at 68% RH.

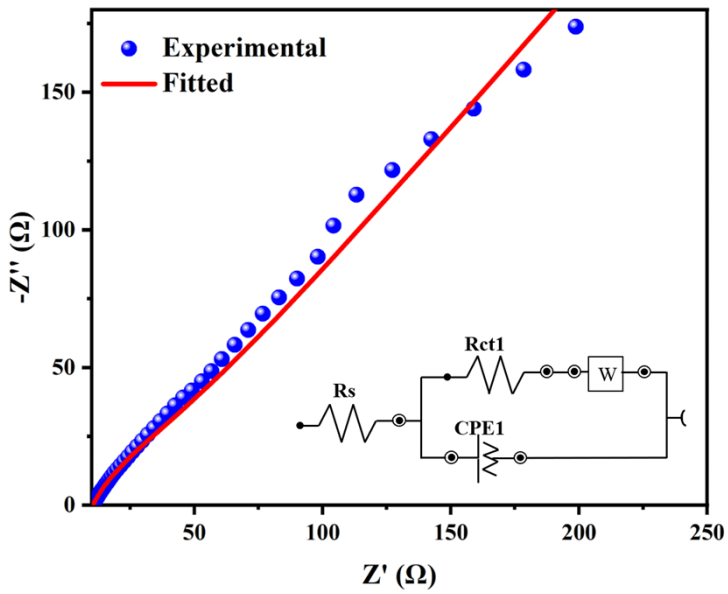

Fig. S22. The simulated Nyquist plot of **Eu-MOF** at 90°C and 98% RH, the insert picture is the equivalent circuits.

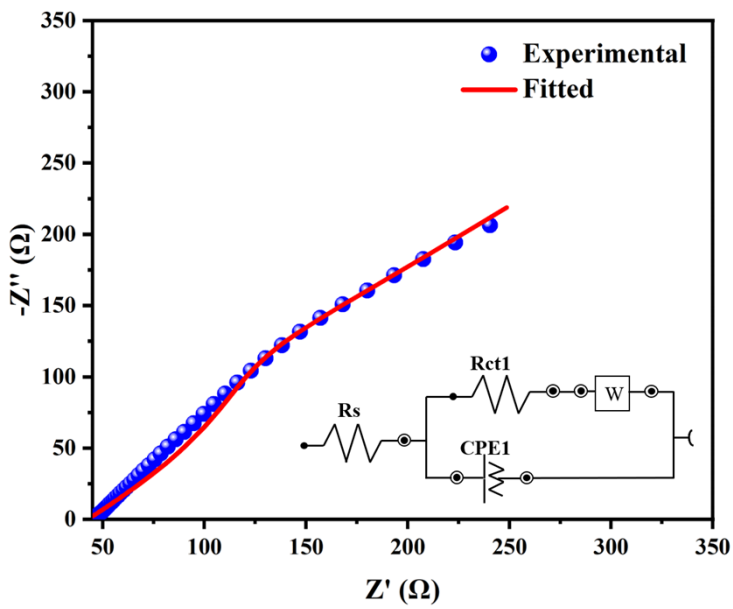

Fig. S23. The simulated Nyquist plot of **Dy-MOF** at 90°C and 98% RH, the insert picture is the equivalent circuits.

Table S1. Crystal data and structure refinement for **Eu-MOF** and **Dy-MOF**.

Compound	**Eu-MOF**	**Dy-MOF**
Formula	$C_{63}H_{52}EuF_4N_3O_{12}$	$C_{63}H_{52}DyF_4N_3O_{12}$
Formula weight	1086.54	1281.57
Temperature (K)	293(2)	150.15
Crystal system	monoclinic	monoclinic
Space group	$P2_1/c$	$P2_1/c$
a (Å)	24.9479(14)	24.9144(15)
b (Å)	9.1728(5)	9.0765(6)
c (Å)	39.8370(17)	39.7778(19)
Volume (Å^3)	7903.1(7)	7782.5(8)
Z	4	4
density (g cm^{-3})	0.913	1.094
F (000)	2112	2596
R_{int}	0.0819	0.0436
R_1, wR_2 [I>=2σ (I)] [a]	0.0485/0.1212	0.0663/0.1624
R_1, wR_2 [all data] [b]	0.0654/ 0.1285	0.0779/ 0.1697
GOF	1.034	1.104

[a] $R_1 = \sum|Fo - Fc| / \sum|Fo|$. [b] $wR_2 = \sum[w(Fo^2 - Fc^2)^2] / w(Fo^2)^2]^{1/2}$

Table S2. Selected bond distances (Å) for **Eu-MOF** and **Dy-MOF**.

Eu-MOF		**Dy-MOF**	
Eu-O1	2.373 (3)	Dy-O1	2.496 (5)
Eu-O2[1]	2.488 (3)	Dy-O2[1]	2.432 (5)
Eu-O3[2]	2.389 (3)	Dy-O3[2]	2.449 (6)
Eu-O4	2.456 (3)	Dy-O4[1]	2.407 (5)
Eu-O5[3]	2.518 (3)	Dy-O5[2]	2.441 (4)
Eu-O6	2.490 (3)	Dy-O6[2]	2.466 (5)
Eu-O7[1]	2.510 (3)	Dy-O9[3]	2.321 (4)
Eu-O9[3]	2.489 (3)	Dy-O10	2.327 (5)
Eu-C7[1]	2.850 (4)	Dy-O11	2.342 (5)
Eu-C24[3]	2.869 (4)	Dy-C7	2.837 (6)
Eu-C25	2.821 (4)	Dy-C27[1]	2.782 (7)
Eu-O0AA	2.392 (3)	Dy-C40[2]	2.813 (6)

Symmetry transformations used to generate equivalent atoms for **Eu-MOF**: [1]1-X, -2-Y, -Z; [2]1-X, 1/2+Y, 1/2-Z; [3]-X, -1-Y, -Z, and **Dy-MOF**: [1]2-X, -Y, -Z; [2]-1+X, 1+Y, +Z; [3]1-X, 1/2+Y, 3/2-Z.

Table S3. Selected angles (°) for **Eu-MOF** and **Dy-MOF**

Eu-MOF		**Dy-MOF**	
O1-Eu-O2^{1}	78.00 (10)	O1-Dy-C7	25.54 (18)
O1-Eu-O3^{2}	82.38 (10)	O1-Dy-C27^{1}	113.64 (19)
O1-Eu-O4	148.53 (10)	O1-Dy-C40^{2}	156.48 (19)
O1-Eu-O5^{3}	79.52 (10)	O2-Dy-O1	51.16 (17)
O1-Eu-O6	151.56 (11)	O2-Dy-O3^{1}	69.8 (2)
O1-Eu-O7^{1}	83.03 (11)	O2-Dy-O5^{2}	139.37 (17)
O1-Eu-O9^{3}	127.70 (11)	O2-Dy-O6^{2}	145.0 (2)
O1-Eu-C7^{1}	78.39 (10)	O2-Dy-C7	25.69 (18)
O1-Eu-C24^{3}	104.46 (11)	O2-Dy-C27^{1}	63.80 (19)
O1-Eu-C25	168.64 (11)	O2-Dy-C40^{2}	152.36 (19)
O1-Eu-O0AA	77.64 (11)	O3^{1}-Dy-O1	109.0 (2)
O2^{1}-Eu-O5^{3}	149.73 (11)	O3^{1}-Dy-O6^{2}	75.6 (2)
O2^{1}-Eu-O6	103.49 (12)	O3^{1}-Dy-C7	88.6 (2)
O2^{1}-Eu-O7^{1}	51.72 (10)	O3^{1}-Dy-C27^{1}	26.4 (2)
O2^{1}-Eu-O9^{3}	137.56 (13)	O3^{1}-Dy-C40^{2}	89.0 (2)
O2^{1}-Eu-C7^{1}	25.75 (11)	O4^{1}-Dy-O1	120.31 (18)
O2^{1}-Eu-C24^{3}	154.71 (11)	O4^{1}-Dy-O2	70.54 (18)

O2^{1}-Eu-C25	91.89 (12)	O4^{1}-Dy-O3^{1}	52.15 (19)
O3^{2}-Eu-O2^{1}	121.79 (10)	O4^{1}-Dy-O5^{2}	73.41 (17)
O3^{2}-Eu-O4	124.74 (10)	O4^{1}-Dy-O6^{2}	92.1 (2)
O3^{2}-Eu-O5^{3}	74.48 (11)	O4^{1}-Dy-C7	95.8 (2)
O3^{2}-Eu-O6	72.69 (10)	O4^{1}-Dy-C27^{1}	26.3 (2)
O3^{2}-Eu-O7^{1}	71.93 (11)	O4^{1}-Dy-C40^{2}	82.52 (19)
O3^{2}-Eu-O9^{3}	97.02 (15)	O5^{2}-Dy-O1	148.31 (19)
O3^{2}-Eu-C7^{1}	96.76 (12)	O5^{2}-Dy-O3^{1}	101.7 (2)
O3^{2}-Eu-C24^{3}	83.28 (11)	O5^{2}-Dy-O6^{2}	52.82 (18)
O3^{2}-Eu-C25	98.91 (12)	O5^{2}-Dy-C7	154.6 (2)
O3^{2}-Eu-O0AA	149.52 (10)	O5^{2}-Dy-C27^{1}	90.7 (2)
O4-Eu-O2^{1}	73.91 (10)	O5^{2}-Dy-C40^{2}	26.3 (2)
O4-Eu-O5^{3}	120.12 (10)	O6^{2}-Dy-O1	143.0 (2)
O4-Eu-O6	52.16 (11)	O6^{2}-Dy-C7	152.3 (2)
O4-Eu-O7^{1}	90.46 (12)	O6^{2}-Dy-C27^{1}	87.0 (2)
O4-Eu-O9^{3}	69.69 (11)	O6^{2}-Dy-C40^{2}	26.5 (2)
O4-Eu-C7^{1}	82.36 (11)	O9^{3}-Dy-O1	78.65 (16)
O4-Eu-C24^{3}	95.24 (11)	O9^{3}-Dy-O2	128.37 (17)
O4-Eu-C25	26.40 (11)	O9^{3}-Dy-O3^{1}	151.29 (18)

O5^{3}-Eu-C7^{1}	157.14 (11)	O9^{3}-Dy-O4^{1}	147.92 (17)
O5^{3}-Eu-C24^{3}	25.52 (10)	O9^{3}-Dy-O5^{2}	78.14 (16)
O5^{3}-Eu-C25	111.75 (11)	O9^{3}-Dy-O6^{2}	82.16 (18)
O6-Eu-O5^{3}	105.95 (12)	O9^{3}-Dy-O10	82.76 (17)
O6-Eu-O7^{1}	76.49 (12)	O9^{3}-Dy-O11	78.24 (18)
O6-Eu-C7^{1}	90.95 (13)	O9^{3}-Dy-C7	103.84 (18)
O6-Eu-C24^{3}	86.31 (13)	O9^{3}-Dy-C27^{1}	167.69 (18)
O6-Eu-C25	26.33 (12)	O9^{3}-Dy-C40^{2}	78.40 (18)
O7^{1}-Eu-O5^{3}	143.79 (12)	O10-Dy-O1	74.68 (17)
O7^{1}-Eu-C7^{1}	26.01 (11)	O10-Dy-O2	93.43 (18)
O7^{1}-Eu-C24^{3}	153.04 (12)	O10-Dy-O3^{1}	73.26 (18)
O7^{1}-Eu-C25	86.64 (12)	O10-Dy-O4^{1}	125.41 (18)
O9^{3}-Eu-O5^{3}	50.89 (11)	O10-Dy-O5^{2}	122.99 (17)
O9^{3}-Eu-O6	70.17 (14)	O10-Dy-O6^{2}	71.73 (18)
O9^{3}-Eu-O7^{1}	146.61 (14)	O10-Dy-O11	149.07 (17)
O9^{3}-Eu-C7^{1}	151.93 (11)	O10-Dy-C7	82.15 (19)
O9^{3}-Eu-C24^{3}	25.57 (11)	O10-Dy-C27^{1}	99.4 (2)
O9^{3}-Eu-C25	63.49 (12)	O10-Dy-C40^{2}	97.3 (2)
C7^{1}-Eu-C24^{3}	177.11 (11)	O11-Dy-O1	77.78 (18)

C25-Eu-C7[1]	90.25 (12)	O11-Dy-O2	79.87 (19)
C25-Eu-C24[3]	86.89 (12)	O11-Dy-O3[1]	130.06 (18)
O0AA-Eu-O2[1]	76.21 (10)	O11-Dy-O4[1]	81.0 (2)
O0AA-Eu-O4	82.11 (11)	O11-Dy-O5[2]	76.60 (17)
O0AA-Eu-O5[3]	79.39 (11)	O11-Dy-O6[2]	128.49 (17)
O0AA-Eu-O6	130.63 (11)	O11-Dy-C7	79.0 (2)
O0AA-Eu-O7[1]	127.19 (10)	O11-Dy-C27[1]	104.4 (2)
O0AA-Eu-O9[3]	77.88 (15)	O11-Dy-C40[2]	102.4 (2)
O0AA-Eu-C7[1]	101.44 (12)	C27[1]-Dy-C7	88.5 (2)
O0AA-Eu-C24[3]	79.75 (11)	C27[1]-Dy-C40[2]	89.3 (2)
O0AA-Eu-C25	105.20 (12)	C40[2]-Dy-C7	177.6 (2)

Symmetry transformations used to generate equivalent atoms for **Eu-MOF**: [1]1-X, 2-Y, -Z; [2]1-X, -1/2+Y, 1/2-Z; [3]-X, -1-Y, -Z, and **Dy-MOF**: [1]2-X, -Y, 2-Z; [2]-1+X, 1+Y, +Z; [3]1-X, 1/2+Y, 3/2-Z; [4]1+X, -1+Y, +Z; [5]1-X, -1/2+Y, 3/2-Z.

Table S4. Proton conductivity of **Ln-MOF** at different RHs and temperatures.

Eu-MOF					
T (°C) /RH (%)	68%	75%	85%	93%	98%
30°C	4.14×10^{-7}	4.16×10^{-7}	2.65×10^{-7}	1.68×10^{-6}	2.68×10^{-5}
40°C	7.34×10^{-7}	1.41×10^{-6}	1.61×10^{-6}	5.42×10^{-6}	1.45×10^{-4}
50°C	2.63×10^{-6}	3.51×10^{-6}	3.95×10^{-6}	1.31×10^{-5}	4.73×10^{-4}
60°C	3.41×10^{-6}	6.58×10^{-6}	1.33×10^{-5}	4.58×10^{-5}	1.76×10^{-3}
70°C	6.76×10^{-6}	1.29×10^{-5}	2.98×10^{-5}	1.13×10^{-4}	1.30×10^{-2}
80°C	1.42×10^{-5}	2.79×10^{-5}	1.00×10^{-4}	3.14×10^{-4}	4.23×10^{-2}
90°C	9.00×10^{-5}	1.59×10^{-5}	2.04×10^{-3}	3.49×10^{-2}	5.35×10^{-2}

Dy-MOF					
T (°C) /RH (%)	68%	75%	85%	93%	98%
30°C	3.99×10^{-9}	5.24×10^{-9}	1.41×10^{-7}	1.12×10^{-7}	1.20×10^{-5}
40°C	1.03×10^{-8}	1.87×10^{-8}	7.53×10^{-7}	2.59×10^{-7}	4.36×10^{-5}
50°C	2.83×10^{-8}	6.65×10^{-8}	2.69×10^{-6}	1.02×10^{-6}	1.73×10^{-4}
60°C	5.68×10^{-8}	1.61×10^{-7}	4.63×10^{-6}	2.52×10^{-6}	3.93×10^{-4}
70°C	1.87×10^{-7}	4.01×10^{-7}	5.97×10^{-6}	0.38×10^{-6}	8.47×10^{-4}
80°C	2.55×10^{-6}	1.74×10^{-6}	9.79×10^{-6}	0.99×10^{-5}	2.12×10^{-3}
90°C	8.61×10^{-6}	8.77×10^{-6}	7.03×10^{-5}	0.78×10^{-4}	1.22×10^{-2}

Table S5. Comparison of σ values between **Ln-MOF** and other MOF.

Compounds	σ value ($S\ cm^{-1}$)	Tested conditions	Ref.
Eu-MOF	**5.35×10^{-2}**	90°C, 98% RH	**this work**
Dy-MOF	**1.22×10^{-2}**	90°C, 98% RH	**this work**
MIP-202(Zr)	1.10×10^{-2}	90°C, 95% RH	5
$[Zr_6O_4(OH)_4(DTD)_6]\cdot5DMF\cdot H_2O$	0.67×10^{-2}	100°C, 98% RH	6
UPC-H9	9.52×10^{-3}	30°C, 80%RH	7
$(Me_2NH_2)_2(H_2O)[EuL_2]\cdot8H_2O$	8.83×10^{-3}	95°C, 60% RH	8
$(Me_2NH_2)[Eu(pmip)]$	3.76×10^{-3}	100°C, 98% RH	9
UiO-66(Zr)-$(CO_2H)_2$	2.30×10^{-3}	90°C, 95% RH	10
$\{[[(CH_3)_2NH_2]_3Eu_2(DTTP\text{-}2OH)_2(HCOO)(H_2O)]\cdot4H_2O\}_n$	1.91×10^{-3}	60°C, 98% RH	11
$(Hdmbpy)[Dy(H_2dobdc)_2(H_2O)]\cdot3H_2O$	1.20×10^{-3}	70°C, 100% RH	12
VNU-15	7.70×10^{-4}	95°C, 40% RH	13
JUK-14	3.60×10^{-4}	60°C, 90% RH	14
$Tb(H_2L)(H_2bts)(H_2O)]\cdot H_2O$	2.30×10^{-4}	95°C, 95% RH	15
$Eu_2(CO_3)(ox)_2)(H_2O)_2\cdot4H_2O$	9.30×10^{-3}	25°C, 40%RH	16
$[Dy(L)(Ox)(H_2O)]_n\cdot1.5H_2O$	9.06×10^{-5}	80°C, 95% RH	17

Reference

[1] F. M. Wang, W. Liu, S. J. Teat, F. Xu, H. Wang, X. L. Wang, L. T. An and J. Li, *Chem. Commun.*, 2016, **52**, 10249-10252.

[2] H. Chen, S.-Y. Han, R.-H. Liu, T.-F. Chen, K.-L. Bi, J.-B. Liang, Y.-H. Deng and C.-Q. Wan, *J. Power Sources*, 2018, **376**, 168-176.

[3] M.-S. Yao, X.-J. Lv, Z.-H. Fu, W.-H. Li, W.-H. Deng, G.-D. Wu and G. Xu, *Angew. Chem. Int. Ed.*, 2017, **56**, 16510-16514.

[4] S. Chand, S. C. Pal, A. Pal, Y. X. Ye, Q. J. Lin, Z. J. Zhang, S. C. Xiang and M. C. Das, *Chem. Eur. J.*, 2019, **25**, 1691-1695.

[5] S. J. Wang, M. Wahiduzzaman, L. Davis, A. Tissot, W. Shepard, J. Marrot, C. Martineau-Corcos, D. Hamdane, G. Maurin, S. Dewautour-Vinot and C. Serre, *Nat. Commun.*, 2018, **9**, 4937.

[6] Y.-L. Hong, Z. H. Xu, J. Du, Z.-Q. Shi, Y.-H. Zuo, H.-L. Hu and G. Li, *Inorg. Chem.*, 2024, **63**, 10786-10797.

[7] Y. J. Wang, M. H. Zhang, Q. Q. Yang, J. B. Yin, D. Liu, Y. X. Shang, Z. X. Kang, R. M. Wang, D. F. Sun and J. Z. Jiang, *Chem. Commun.*, 2020, **56**, 15529-15532.

[8] S. L. Zhang, Y. X. Xie, M. R. Yang and D. R. Zhu, *Inorg. Chem. Front.*, 2022, **9**, 1134.

[9] Y.-S. Wei, X.-P. Hu, Z. Han, X.-Y. Dong, S.-Q. Zang and T. C.W. Mark, *J. Am. Chem. Soc.*, 2017, **139**, 3505-3512.

[10] D. B. Daiane, D.-V. Sabine, J. Herve, O. Jacques, N. Farid, S. Rocio, D. Thomas, S. Christian, P. Francesco and M. Guillaume, *Angew. Chem. Int. Ed.*, 2016, **55**, 3919-3924.

[11] J.-J. Hu, K. L. Xie, T.-Z. Xiong, M.-M. Wang, H.-R. Wen, Y. Peng and S.-J. Liu, *Inorg. Chem.*, 2023, **62**, 12001-12008.

[12] F.-G. Chen, W. Xu, J. Chen, H.-P. Xiao, H.-Y. Wang, Z. Y. Chen and J.-Y. Ge, *Inorg. Chem.*, 2022, **61**, 5388-5396.

[13] T. N. Tu, N. Q. Phan, T. T. Vu, H. L. Nguyen, K. E. Cordova and H. Furukawa, *J. Mater. Chem. A*, 2016, **4**, 3638.

[14] M. Szufla, A. Choroś, W. Nitek and D. Matoga, *Chem. Eur. J.*, 2022, **28**, 37.

[15] Y.-N. Zhou, L.-L. Liu, Q.-W. Liu, X.-X. Liu, M.-Z. Feng, L. Wang, Z.-G. Sun, Y.-Y. Zhu, X. Zhang and C.-Q. Jiao, *Inorg. Chem.*, 2021, **60**, 17303-17314.

[16] Q. Tang, Y. W. Liu, S X. Liu, D. F. He, J. Miao, X. Q. Wang, G. C. Yang, Z. Shi and Z. P. Zheng. *J. Am. Chem. Soc.*, 2014, **136**, 12444-12449.

[17] H. Wu, F. Yang, X.-L. Lv, B. Wang, Y.-Z. Zhang, M.-J. Zhao and J.-R. Li, *J. Mater. Chem. A*, 2017, **5**, 14525-14529.